



Article

Considerations and Multi-Criteria Decision Analysis for the Installation of Collocated Permanent GNSS and SAR Infrastructures for Continuous Space-Based Monitoring of Natural Hazards

Dimitris Kakoullis ^{1,2,*} , Kyriaki Fotiou ^{1,2}, George Melillos ^{1,2} and Chris Danezis ^{1,2}

¹ Department of Civil Engineering & Geomatics, Cyprus University of Technology, Limassol 3036, Cyprus; kyriaki.fotiou@cut.ac.cy (K.F.); georgios.melillos@cut.ac.cy (G.M.); chris.danezis@cut.ac.cy (C.D.)

² ERATOSTHENES Centre of Excellence, Limassol 3036, Cyprus

* Correspondence: dimitris.kakoullis@cut.ac.cy

Abstract: Over the past few decades, the global population and the built environment's vulnerability to natural hazards have risen dramatically. As a result, decisive actions, such as the SENDAI framework, have emerged to foster a global culture of successful disaster risk reduction policies, including actions to mitigate the social and economic impact of geohazards. The effective study of natural disasters requires meticulous and precise monitoring of their triggering factors, with ground- and space-based techniques. The integration of GNSS and SAR observations through the establishment of permanent infrastructures, i.e., Continuously Operating Reference Stations (CORS) networks and arrays of Corner Reflectors (CRs), may form a seamless ground displacement monitoring system. The current research literature provides fragmented guidelines, regarding the co-location of SAR and GNSS permanent infrastructures. Furthermore, there exist no guidelines for the determination of the most suitable locations using a holistic approach, in terms of criteria and required data. The purpose of this paper is to present a semi-automatic multicriteria site suitability analysis and evaluation of candidate sites for the installation of a permanent CORS and two CRs; one for each pass, taking into account various parameters and criteria. The first results demonstrate that the collocation of SAR and GNSS permanent infrastructures, utilizing a holistic criteria-based approach, is successful and complies with all the literature's requirements.

Keywords: natural hazards; GPS; GNSS; InSAR; corner reflector; Multi-Criteria Decision Analysis; infrastructures



Citation: Kakoullis, D.; Fotiou, K.; Melillos, G.; Danezis, C. Considerations and Multi-Criteria Decision Analysis for the Installation of Collocated Permanent GNSS and SAR Infrastructures for Continuous Space-Based Monitoring of Natural Hazards. *Remote Sens.* **2022**, *14*, 1020. <https://doi.org/10.3390/rs14041020>

Academic Editor: Alex Hay-Man Ng

Received: 29 December 2021

Accepted: 17 February 2022

Published: 20 February 2022

Publisher's Note: MDPI stays neutral with regard to jurisdictional claims in published maps and institutional affiliations.



Copyright: © 2022 by the authors. Licensee MDPI, Basel, Switzerland. This article is an open access article distributed under the terms and conditions of the Creative Commons Attribution (CC BY) license (<https://creativecommons.org/licenses/by/4.0/>).

1. Introduction

The collocation of permanent infrastructures, such as GNSS continuously operating reference station (CORS) networks and Interferometric Synthetic Aperture Radar (InSAR) Corner Reflectors (CRs) arrays, represents the state of the art, in terms of dedicated sensors for seamless space-based monitoring of geohazards, towards the fulfilment of important incentives on disaster risk reduction, such as the SENDAI framework [1]. GNSS can record 3D position changes of a single point on the physical surface with an accuracy of a few millimetres [2]. InSAR techniques offer 2-dimensional surface deformation trends with greater spatial resolution [3]. Although, one of the main advantages of InSAR is that it does not require advanced planning or in-situ markers, as the use of CRs is mandated to improve spatial sampling in areas poor of persistent scatterers (PS) and to connect InSAR with other techniques, such as GNSS [4]. Therefore, the two space-based techniques can be combined by determining a known displacement rate, generated from GNSS, to an InSAR 2D image and assigning both products to the same reference [5]. The collocation between the GNSS antenna and the CRs brings GNSS and InSAR to a common reference frame,

promotes the precision of InSAR measurements and, hence, the reliability of deformation products [6,7].

A new co-located GNSS/SAR infrastructure has been established in Cyprus, in the framework of the CyCLOPS project (Cyprus Continuously Operating Natural Hazards Monitoring and Prevention System) [8]. This project revolves around the formation of a strategic research infrastructure unit for geohazard monitoring, in Cyprus and the South-eastern Mediterranean Region. CyCLOPS is comprised of permanent collocated multi-sensor configurations, spread throughout the country for monitoring geohazards and solid earth processes. CyCLOPS is formed of the following two major parts: a novel multiparametric network (MPN) of sensors and an operation center (OC). The MPN consists of two segments (permanent and mobile). The permanent segment includes cutting-edge high-rate permanent GNSS receivers, which are installed at specifically selected sites on top of highly stable monuments, anchored in bedrock, according to the most stringent specifications (UNAVCO, IGS, and EPN guidelines). The collocated configuration of GNSS CORS and CRs is realized to be compliant with (a) all current GNSS constellations (GPS, GLONASS, Galileo, BeiDou-3) and (b) the current space-based SAR missions, such as Copernicus Sentinel-1 and TerraSAR-X. To date, six permanent sites have been established in government-controlled areas the Republic of Cyprus (depicted in Figure 1). In each site, two CRs (one for ascending and one for the descending pass) and one GNSS CORS are collocated, taking into account numerous and significant parameters, such as sky visibility, security, land topography, geology formation, land ownership, land cover, land access, and the backscatter coefficient (σ_0).

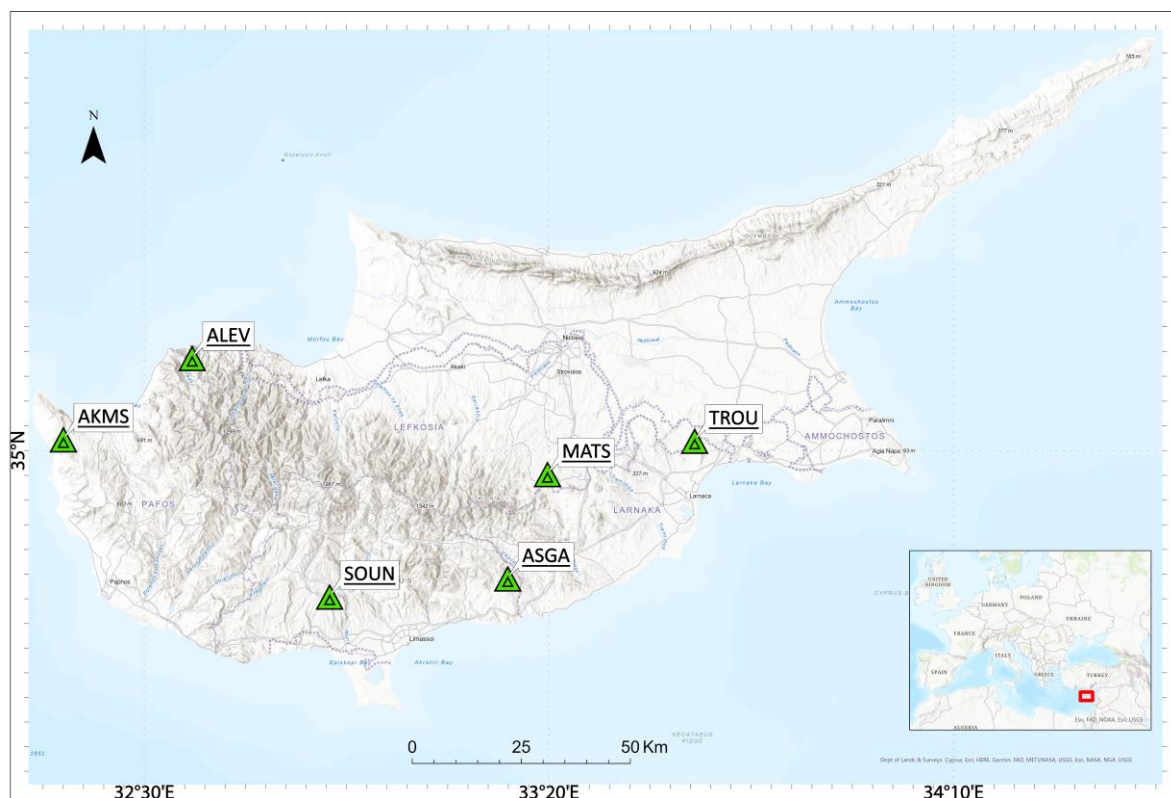


Figure 1. Site Locations of the Permanent Segment. Green triangles indicate the reference stations.

One of the major challenges faced in the establishment of CyCLOPS was the determination of the most suitable locations for the installation of sensors. Generally, the use of a GNSS CORS, in close proximity to artificial Persistent Scatterers (PS), such as CRs, serves as a valuable confirmation tool to the PS-estimated displacements [6]. However, the CRs should be installed in such a way, that the GNSS signal is not affected mainly by multipath.

Moreover, the GNSS reference station, should be installed at sites that strictly adhere to strict guidelines set by world renowned services (IGS, UNAVCO, EPN), which require increased monument stability to isolate the station from surface soil movement and, thus, avoid the introduction of biases in the estimation of displacements.

In the current scientific literature on the collocation of GNSS/InSAR infrastructures, there are no specific guidelines or methodology for the determination of the most suitable locations, using a holistic approach in terms of criteria and required data.

Therefore, the objective of this paper is to propose and present a semi-automatic multicriteria analysis and evaluation of candidate sites for the installation and collocation of a permanent GNSS CORS and a pair of InSAR CRs, one for each pass, taking into account the crucial parameters that affect not only their individual localization but also their interspatial relationship.

2. Materials and Methods

The workflow for the determination of the collocated GNSS CORS/InSAR CRs that was followed in the case of CyCLOPS infrastructure can be summarized in the following steps:

- (a) Meetings with the competent authorities for the identification of candidate locations;
- (b) Initial assessment of the candidate location (visual inspection of site suitability in terms of geological background and natural or man-made obstructions);
- (c) Terrestrial and Airborne Surveying of the candidate location and acquisition of a 24 h sample dataset of GNSS observations.
- (d) Analysis of GNSS dataset (e.g., multipath, satellite availability) along with UAV and SAR image processing;
- (e) Suitability Analysis and Determination of candidate GNSS and CR locations;
- (f) Validation of the Suitability Analysis results and finalization of site selection;
- (g) Acquisition of official permits (i.e., lease) from the competent authorities.

The suitability analysis (step e) proposed in this research was carried out in the following stages:

- (1) Determination of Criteria and Constraints
- (2) Multi-Criteria Decision Analysis (MCDA)
 - a. Analytic Hierarchy Process (AHP) Analysis
 - b. Weighted Overlay (WO) Analysis
- (3) 3D Visibility Analysis

The determination of the criteria and constraints that are involved in the proposed methodology was based on the guidelines of the responsible institutions for GNSS (i.e., IGS, UNAVCO, EPN) and the latest scientific literature on CR installation. Consequently, the criteria were categorized and classified based on the importance of one over another, using MCDA. The latter includes the following two subprocesses: (a) the AHP analysis, which was used to derive ratio scales from the criteria, and (b) the WO analysis. The number of candidate locations was then substantially reduced by applying constraints based on significant parameters, such as the underlying geology, the area ownership (state land), and others. The result of the analysis is an extracted raster layer of the most suitable locations, categorized according to the degree to which they conformed to the specified criteria. Moreover, a 3D visibility analysis is also included in the process to finalize the selection of the most suitable locations. Hence, Line of Sight (LOS) and the distance between the two CRs were checked along with the inter-visibility and distance between the GNSS antenna and CRs (for the mitigation of unwanted multipath in GNSS observations). Finally, the average incidence angle for ascending and descending passes were also considered to account for the baseplate elevation angle of the CR. The flowchart of the semi-automatic suitability analysis procedure for the determination of CRs' final locations is illustrated in Figure 2. Each step is analysed further in the following sections.

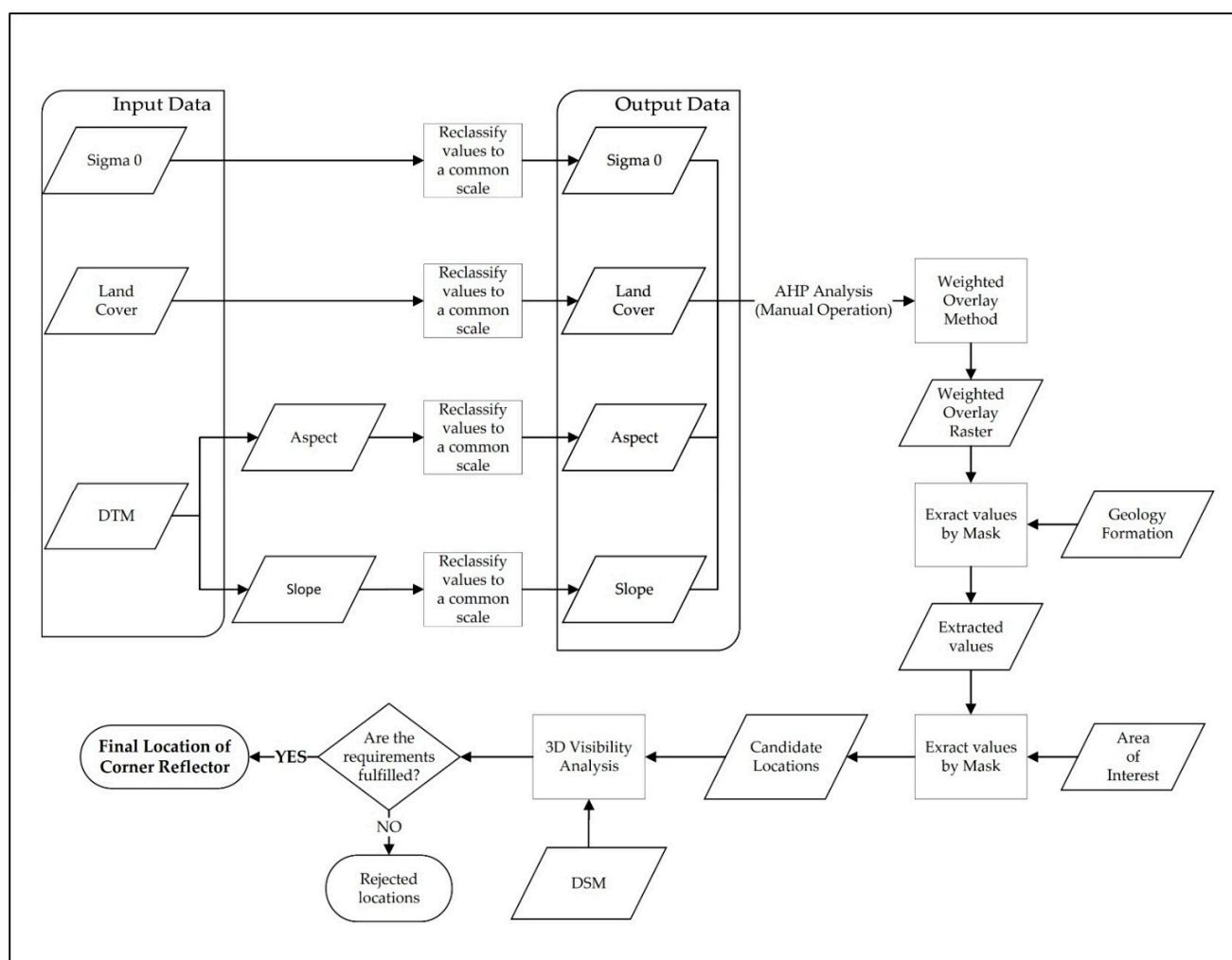


Figure 2. The suitability analysis procedure for the determination of the CRs' final location.

2.1. Determination of Site Suitability Criteria and Constraints

All the candidate sites should be located in government-controlled areas (parcels). Since CyCLOPS is a strategic infrastructure, and the objective is to provide nationwide coverage, CUT cooperated with the Department of Lands and Surveys (DLS) to determine candidate state parcels within the Republic of Cyprus. The selection was refined and finalized after consulting with the Geological Survey Department (GSD), and taking into account crucial information on Cyprus's geological, geodynamic, and geotechnical regime. The acquisition of official site permits, including the required works for equipment safety (i.e., fencing), was mandatory for installing the permanent segment. The choice of state land was obvious, since the infrastructure has a strategic nature (nationwide coverage), it has to be permanent, and has to provide continuous monitoring. The choice of state land minimises the risk of having to uninstall or move the infrastructure due to ownership changes, through long-term lease of the government parcels.

Evidently, the site selection process must fulfil all the requirements and criteria to maximise both GNSS and CRs performance. A review of the most critical performance factors per sensor follows.

2.1.1. GNSS CORS Installation Requirements

According to the CORS guidelines released by the Intergovernmental Committee on Survey and Mapping (ICSM) [9], GNSS CORS are divided into three categories in terms of the station's purpose and stability (i.e., Tier-1, -2, and -3). CyCLOPS has deployed

Tier1/2 GNSS CORS. According to UNAVCO, IGS, and EPN [10–12], such a site should fulfil specific requirements to achieve maximum accuracy during measurements:

- Highly Stable monumentation (on bedrock);
- Open Sky visibility (increased satellite availability);
- Avoidance of potential Radio Frequency Interference (RFI) sources;
- Security from unauthorized access;
- Clear of reflecting surfaces (e.g., fences, metal poles);
- Ease of access;
- Data Accessibility;
- No local crustal instabilities-controlled vegetation;
- Power Supply and energy redundancy;
- Internet connectivity (through wired or wireless broadband internet);
- Augmentation of the existing national networks (filling the gaps for the availability of network solutions).

The requirements mentioned above are vital to the operation and reliability of the GNSS CORS. Since the objective of CyCLOPS was the deployment of Tier1/2 GNSS reference stations, having very stable monuments installed on solid bedrock was the most critical requirement. Following GSD suggestions, an in-situ visit has been carried out in each one of the candidate locations. The objective was to (a) inspect the geological background, (b) verify whether the locations fulfil the above-mentioned site selection requirements, (c) check on the existence of physical or man-made obstacles that can compromise sensor performance and (d) detect potential security threats. After the initial inspection visit, 24-h GNSS data acquisition campaigns were carried out in each candidate location to assess actual GNSS satellite availability, signal quality, multipath and potentially detect signal jamming sources. The datasets were collected using Trimble R9s receivers equipped with Zephyr Geodetic 2 and 3 antennas. The analysis was then processed with G-Nut/Anubis, which has been developed by the Geodetic Observatory Pecny and is the standard software used in the European Plate Observing System (EPOS) EU ESFRI [13].

The results from the analysis allow for the assessment of the data quality for each satellite system (GPS, GLONASS, GALILEO, BeiDou and QZSS) which is tracked from a particular location. The related quality metrics that have been computed from the daily GPS/GNSS datasets at the candidate locations include the following: multipath maps, number of tracked satellites per epoch, histograms of phase measurements per elevation angle of tracked satellites, number of observations per epoch or satellite, number of cycle slips and ambiguities, measurement precision for each satellite arc, estimated receiver clock corrections and their precision, standard deviation of the estimated kinematic coordinates and RMS of the final PPP-estimated coordinates. An example of these metrics for the candidate site ALEV is illustrated in Figure 3.

2.1.2. Triangular Trihedral Corner Reflector (CR) Installation Requirements

The CR is made of aluminum, which is more expensive than steel; however, the structure's weight is much lighter than iron or steel and is notable for its low density, corrosion resistance, and tolerance to oxidization. The use of corner reflectors as coherent targets is considered an advantage due to the conceptually simple and economic construction. Also, CRs do not require a source of power or any electronic components that could affect or decay their performance over time. Nevertheless, periodic maintenance is needed since they are exposed to weather conditions (e.g., snow, rain, high temperatures, strong winds, etc.), fauna, vandalism, or theft during long-term measurements or site occupations [14]. Additionally, CRs, due to their large size, have a significant weight (especially C-band compliant CRs); thus, they need to be strongly mounted and anchored to the ground. The mount should enable orientation flexibility in elevation and azimuth, and it is usually fixed to a partially buried concrete base of sufficient dimension to ensure stability in typical weather conditions.

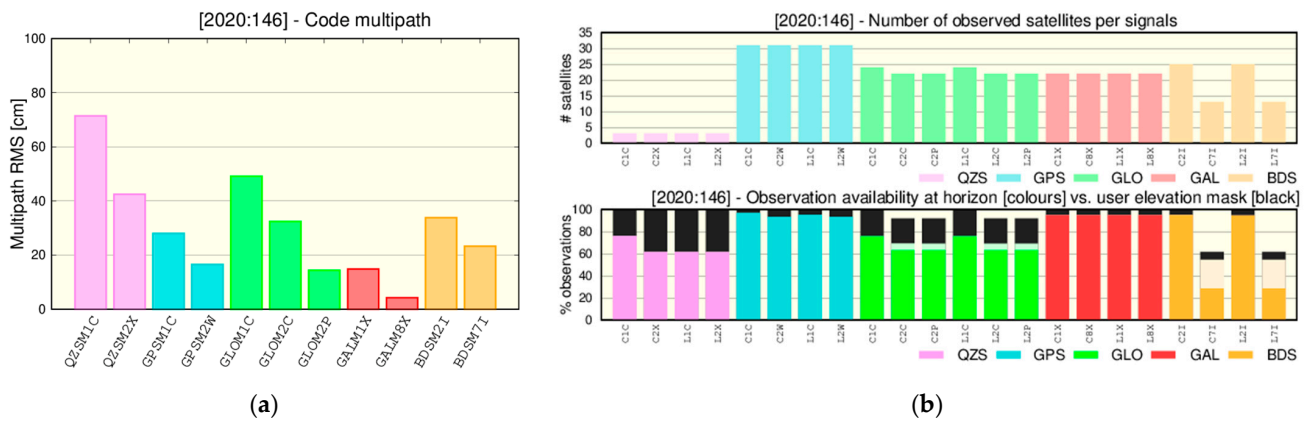


Figure 3. (a) Multipath graph at ALEV site for 24 h data acquisition, with an elevation cut-off angle of 0 degrees; (b) Observation availability of the tracked signals transmitted from each satellite at different elevation angles.

Various types of CR exist, ranging from a single flat plate to dihedrals (2 orthogonal plates), trihedral (3 orthogonal plates) and more exotic configurations [15]. A permanently deployed CR intended for use with various sensors at different wavelengths should be sufficient size to satisfy minimum RCS requirements at a longer wavelength. According to Brock and Doerry [16], the magnitude of RCS is influenced by the size and the shape of the corner reflector; thus, some of the major components being used are flat plate, dihedral and trihedral, while the latter is categorized by the following four types: square, cubic, circular and triangular trihedral. Although the triangular trihedral CR has the lowest RCS of all the mentioned reflector shapes, it is the most commonly used due to its structural rigidity, installation simplicity, requirement of less material to manufacture and it is cheaper [17]. A triangular trihedral side length of 1.5 m is generally suitable for C-, L-, and X-Bands. For optimal performance, it must be re-aligned each time a different sensor makes an acquisition [18]. This can be avoided by aligning the CR in the average direction of the sensors and using a triangular trihedral whose RCS is less affected by misalignments. Fortunately, SAR satellites tend to be in sun-synchronous polar orbits with very similar ground headings and azimuth alignment requirements. In order to be useful for both the ascending and descending passes of a satellite, two CRs are necessary with roughly opposite azimuth orientations.

The RCS of a CR is proportional to the fourth power of its physical size and inversely proportional to the square of the wavelength, λ . Typical SAR sensors operate at X-Band ($\lambda = 3.1$ cm, TerraSAR-X, COSMO-SkyMed, TanDEM-X), C-band ($\lambda = 5.6$ cm, Sentinel-1A/B, RADARSAT-2, RCM) and L-band ($\lambda = 23.5$ cm, ALOS-2/PALSAR-2, SAOCOM-1, NISAR-L) [19]. The RCS of a CR is then smaller at L-Band than at X-Band; nonetheless, this can be compensated for by increasing the size of the corner reflector [20]. Based on the above, the CR type used in CyCLOPS was decided to be the triangular trihedral with an inner length dimension of 1.5 m to support all current SAR missions.

The RCS changes depend on its azimuth orientation and elevation angles; hence, when deployed, the CR should be oriented in such a way that the azimuth and elevation of the boresight vector (originated from the intersection of the three triangular plates) is directed in the SAR satellite's line of sight [16].

A triangular trihedral CR can be considered as an object whose RCS is determined by its open face. The maximum RCS direction is determined as normal to the CR's open face. Concordantly, the orientation angle is expressed as follows:

$$\theta = \frac{\pi}{4} \text{ or } 45^\circ \quad (1)$$

The radar wave is normal to the open face when the elevation angle with one of the side plates is as follows (see Figure 4a) [21]:

$$\psi = \tan^{-1}\left(\frac{1}{\sqrt{2}}\right) \text{ or } 35.26^\circ \quad (2)$$

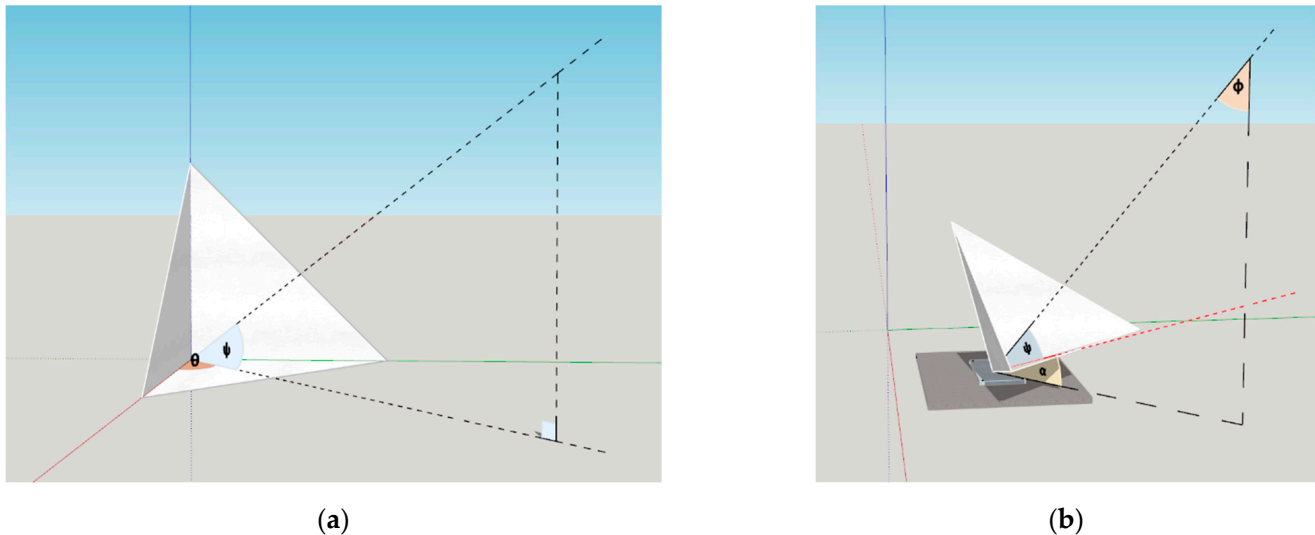


Figure 4. (a) Geometry of a triangular CR. θ represents the azimuth angle and ψ the elevation angle; (b) Adjustment of a triangular trihedral CR. ψ represents the elevation angle, Φ the off-nadir angle, and α the CR tilt angle from the base plate.

Hence, as shown in Figure 4b, for a given incidence angle Φ , the CR must be tilted at an angle α from the baseplate to acquire the maximum RCS.

The most demanding process in this task was the selection of the appropriate locations that would host the aforementioned equipment and would comply with the literature guidelines. According to the literature [17,22,23], numerous parameters should be examined when selecting an installation site for a target to be visible above the background signal level, called clutter. The requirements used for the analysis are presented in Table 1. Besides sigma 0 and the incidence angle, the remaining factors can also be used as criteria for choosing the most suitable GNSS location. The incidence angle is needed for the calculation of the CR's baseplate elevation angle to perform the maximum RCS.

Table 1. The requirements used for the suitability analysis.

Criteria (Factors)	Favourable Values
Backscatter coefficient (sigma 0)	≤ -10 dB (at C-band)
Land Cover	Stable solid surface, no dense vegetation, and trees, no metallic structures
Slope	$< 10^\circ$
Land Ownership	Government control area
Geological Formation	No marls, clays, sand, silts, or gravel
Ground Surface Aspect	Flat, or Oriented toward the direction of the satellite pass
Distance between CRs and CORS	Distance between GNSS antenna and CRs > 30 m with no inter-visibility.
Incidence Angle	Distance between the 2 CR sites > 200 m The radar signal's average incidence angle with the target

As shown in Table 1, the main criteria for selecting the most suitable location for a CR are sigma 0 (σ_0), land cover, slope, and aspect. For a CR installation to be considered successful and operational, the sigma 0—the normalized measure for determining the intensity of radar signals reflected by a distributed scatterer in an SAR image—must be less

than -10 dB at C-band [22,24]. Land cover near CRs should be free of dense vegetation and trees, as well as man-made structures, and the surface should be stable and solid. The slope in the installation area should not exceed 10° , and the ground surface aspect should be oriented as much as possible toward the direction of the satellite pass [23]. These criteria and constraints are using the stage of the MCDA.

2.2. Multi-Criteria Decision Analysis (MCDA)

MCDA is the process concerned with allocating land to meet a specific goal based on various attributes that the chosen places should have, and in order to succeed, the evaluation process must be based on accurate data [25]. The criteria selection is one of the most crucial processes, which depends on data availability. The data required for the proposed research were acquired by UAV site mapping missions of the areas of interest, and from state authorities (GSD, DLS).

2.2.1. Site Mapping Using UAV

Each site was surveyed using a tactical-grade Unmanned Aerial Vehicle (UAV), the SenseFly eBee X RTK, which is able to perform direct in-flight georeferencing using two-frequency Real-Time Kinematic (RTK) positioning. For every site, the following products were generated, using PIX4D Mapping Software version 4.6.4: (a) a 2D orthomosaic, (b) a high-resolution Digital Terrain Model (DTM), (c) a high-resolution Digital Surface Model (DSM), (d) Contour Maps, (e) a Photorealistic 3D model. Digital elevation models are commonly used as a data source for spatial analysis because they represent the constantly changing topographic surface [26]. These products aim to obtain slope, aspect, and land cover data and enable LOS visibility and exploratory analysis. The main purpose of the UAV mapping was the creation and validation of models to enable the determination of the final locations of GNSS CORS and CRs. The derivation of the required products was based on the following steps:

UAV flight planning was carried out using the eMotion Software version 3.12.0 (see Figure 5). During this step, weather conditions, altitude, possible take-off and landing areas have been checked. Additionally, a block with photo overlaps and sidelaps was planned in order to have an adequate overlap between images (latitude 75%, longitude 85%) [27]. Moreover, the total time of flight, the direction of the UAV, and the battery charging levels were estimated to simulate the entire process prior to moving outdoors.



Figure 5. Flight Planning using the eMotion Software.

Consequently, the CyCLOPS team proceeded with the airborne mapping of the candidate areas in order to create high-resolution georeferenced 2D and 3D products. The fixed-wing eBee X was equipped with a GNSS receiver capable of measuring with the RTK method, achieving a centimetre-level accuracy without using ground control points and covering areas up to 500 hectares (5 Km²) in 90 min of flight. The UAV is equipped with senseFly SODA 3D mapping camera (sensor 1", RGB resolution 5472 × 3648 px (3:2)), which has the ability to change orientation during flight to acquire three images (one nadir, and two obliques) each time [28], as shown in Figure 6. In this sense, it obtains a much wider field of view, ensuring excellent 3D mapping results in vertically focused environments; thus, it is suitable for large-scale aerial mapping.

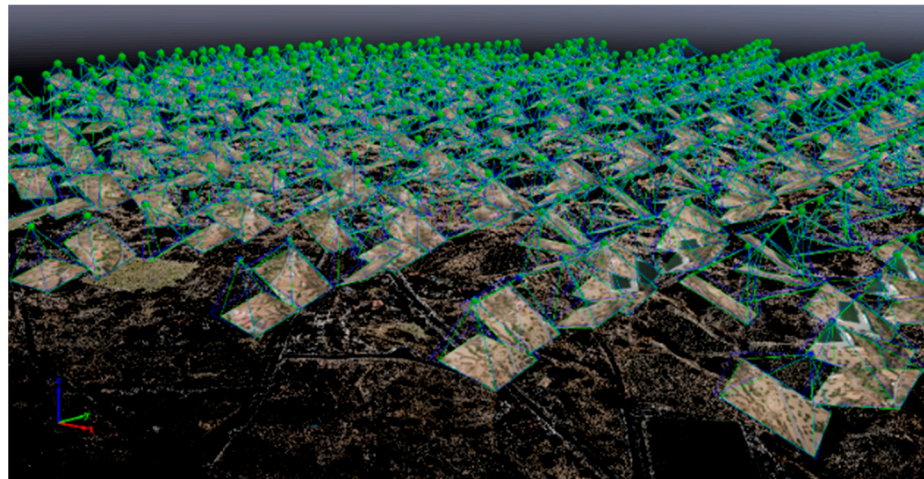


Figure 6. The produced point cloud from the acquired images (one nadir and two obliques).

The point cloud, which was generated using the imported images in Pix4D software, is a set of 3D points modelling reconstruction. The densified point cloud is computed based on the automatic tie points (ATPs) of the initial processing, which contains the following: (a) matching image pairs that allow the selection of which pair of the images are combined and (b) matching strategy for the determination of how the images are matched. Thus, it provides a very accurate background for distance, surface, and volume measurements. Note that the primary products, which have been created through the airborne mapping process are DSM, DTM, and Orthomosaics with a spatial resolution of 2.50 cm/pixel, respectively. These products provide the required criteria via a GIS-based process.

2.2.2. GIS-Based Derivation of Criteria and Constraints

Using ESRI's ArcGIS Pro, the desired raster images of slope and aspect were created from DTM, whilst the land cover data were created from the orthomosaic performing a supervised classification. All the generated products were applied for the finalization of the GPS/GNSS stations' location and the multicriteria analysis for the Corner Reflectors' site selection. In addition, the geological background vector data and the boundaries of each candidate government-controlled area were added to the GIS environment, and finally, backscatter coefficient raster images were included in the software. The explanation of the above data's generation is presented in detail below. Note that while the approach used in the ALEV location is described in this article, the same procedure was used for the finalization of the points of interest at each site.

Slope

The slope map of a terrain identifies the steepness at each raster cell. The terrain becomes steeper as the slope value is increased and vice versa [29]. As mentioned in Section 2.1.2, the most favourable terrain for installing a CR is a surface with less than 10 degrees of steepness. The slope criterion was created from DTM and categorized into

three variables (≤ 5 , 5–10, and 10–90 degrees of steepness (see Figure 7). The reason for this classification is that a flat terrain ($\leq 5^\circ$) is the most beneficial value for equipment installation; nevertheless, if the latter does not match the other criteria, terrain with a slope of up to 10° will be selected. All additional values ($\leq 90^\circ$) were categorized for the sake of visualization and were excluded from the analysis.



Figure 7. Output slope raster (in degrees). White colour indicates terrain with ≤ 5 , light brown ≤ 10 , and dark brown ≤ 90 of steepness.

Aspect

The aspect map determines which direction the slope is facing. It is measured clockwise, making a full circle from 0° (North) to 360° ; moreover, a flat terrain has no downslope direction, thus, is assigned the rating of -1 [30]. Figure 8 shows the output aspect criterion with the generated values of North, Northeast, East, Southeast, South, Southwest, West, and Northwest visualized in different colours (see Table 2).

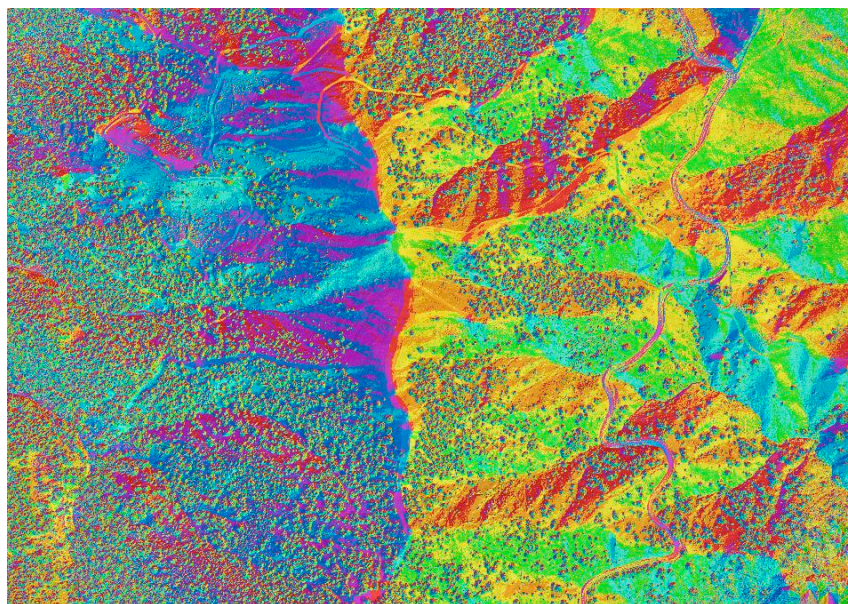


Figure 8. Output aspect raster map. Each colour indicates the slope facing direction.

Table 2. The generated values from the aspect raster map and the way they are visualized in Figure 8.

Aspect Direction	Values (Degrees)	Colour
Flat	−1 ¹	Grey
North	0–22.5	Red
Northeast	22.8–67.5	Orange
East	67.5–112.5	Yellow
Southeast	112.5–157.5	Light Green
South	157.5–202.5	Cyan
Southwest	202.5–247.5	Blue
West	247.5–292.5	Dark Blue
Northwest	292.5–337.5	Purple
North	337.5–360	Dark Red

¹ No downslope direction.

Sentinel-1 satellite mission is a near-polar, sun-synchronous orbit, performing C-band synthetic aperture radar imaging [31]; both ascending and descending pass directions are available in Cyprus. In particular, ascending refers to the satellite's pass from South to North and descending from North to South, where observations are performed from West and East, respectively [32]. Hence, installing the CRs (one for each pass), the aspect direction of East is the most favourable value for the descending pass and West aspect values for the ascending. Flat areas having no downslope direction are also suitable for both passes.

Land Cover




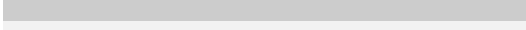

The orthomosaic generated from the images of UAV missions gives a detailed view of the land cover of the AOL. However, to assign the necessary values to the suitability analysis, the raster image must be defined in a land cover classification system to all pixels; ergo, as illustrated in Figure 9, five classes were generated using the supervised classification method. The latter approach relies on manually determined training samples, where the classifier assigns the image pixels to a given class by comparing the classified image with the samples [33].



Figure 9. Output land cover map. Each colour indicates the classified values.

The resulting classified dataset (see Table 3) is a set of values categorized into classes and used as variables of land cover criterion in the suitability analysis.

Table 3. The classified values of the land cover map.

Class Name	Colour
Tree	
Bush	
Soil	
Exposed rock	
Road hard surface	

Each SAR image cell records the amplitude of the signal backscattered toward the radar by the scatterers. This amplitude is determined by the roughness of the terrain rather than the chemical characteristics of the scatterers. Urban areas and surface rocks generally have strong amplitudes, whilst smooth flat surfaces have small amplitudes because the signal is reflected chiefly away from the radar [34]. Hence, the most favourable value for installing a CR is a flat soil surface with no dense vegetation and exposed rocks.

Sigma 0 (σ_0) Criterion

As discussed in Section 2.1.2, finding a suitable location for a CR to be visible above the clutter is crucial. Clutter's magnitude depends on the land cover type, the SAR resolution, the signal incidence angle, wavelength, and polarization. According to Garthwaite et al. [22], a site with a clutter level at C-band within the range -10 dB to -14 dB is suitable for CR installation.

Sigma 0 was calculated from Sentinel 1 ascending (160A) and descending (167D) relative orbit directions over Cyprus. Level-1 Single Look Complex (SLC) products with Interferometric Wide swath (IW) mode and VV single-polarization were used. The images were imported and analyzed using SNAP software, and the generated images are illustrated in Figures 10 and 11.

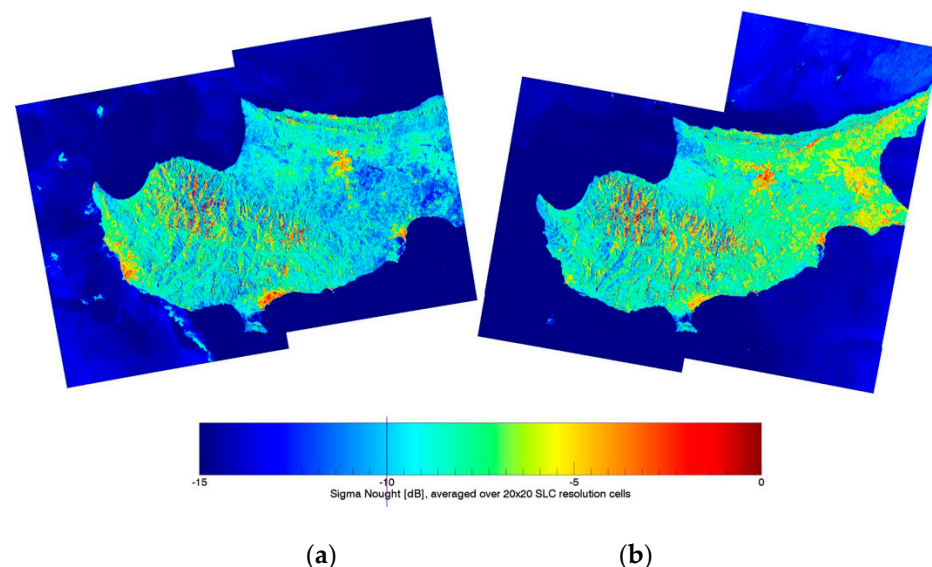


Figure 10. The generated sigma 0 images. (a) The values acquired from the ascending pass; (b) The values acquired from the descending pass. The purple line designates the suitable sigma 0 value of a Sentinel 1-SLC product. Lower values are more favourable.

The reason for the above-mentioned SAR image product selection is because according to ESA [35], (a) the principal acquisition mode over land is IW swath, (b) SLC products preserved phase information and are processed at the natural pixel spacing, and (c) as regards the single polarization choice, trihedral CR returns linearly polarized incident waves unchanged [36]; thus, it will only have a response in a single polarization.

After making the sigma 0 images in SNAP, they were imported into ArcGIS Pro. Subsequently, a subset of the images was overlaid on each DSM's area of interest to see

how it appears at first glance related to the 3D visualized terrain. Figure 11 illustrates the sigma 0 raster image overlaid on the ALEV's DSM.

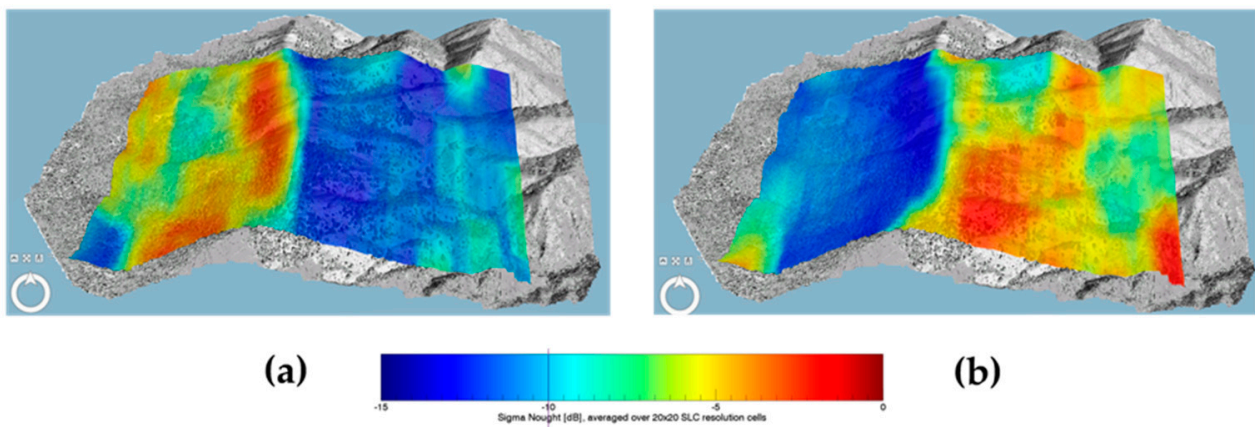


Figure 11. Sigma 0 images overlaid on ALEV DSM. (a) The subset of the ascending pass; (b) The subset of the descending pass. The sigma 0 most favourable values are depicted from purple to blue colour.

The sigma 0 values from the ascending and descending raster images will be used as variables of the criterion “Sigma 0” to determine the suitability of CR’s permanent installation for the ascending and descending passes, respectively. The most favourable variables were the values less than -10 dB, whereas the values equal to or greater than 0 dB were excluded from the analysis.

Reclassification of the Raster Images

In the reclassification process, the pixels of a specific value are identified and reclassified to a new value, set by the user [37]. In weighted site selection, reclassification is vital because it simplifies the interpretation of raster data by converting a single input value into a new output value [38]. Since the above-mentioned input criteria will be in multiple and different numbering systems, with varying individual (e.g., land cover) and range values (e.g., slope), they must be reclassified into a common scale before being combined for use in a single suitability analysis.

Specifically, as depicted in Table 4, under the slope criterion, values in the range of 0 to 5 degrees are reclassified with the new value 1; input values in the range of 5 to 10 degrees are assigned to the output value 2, and so forth. The two aforementioned ranges have as an input value the number 5; ergo, in the first range, an input value less than or equal to 5 will be assigned to 1, while in the second range an input value greater than 5 (e.g., 5.01), will be assigned to 2 to avoid overlapping. Different values in the same criterion need to be restricted for the suitability analysis, while others must be determined as favourite values; thus, they are assigned to the same value.

For the ascending pass, the aspect input values of East are assigned to the same values as the North and South aspects. Contrarily, West input values are assigned to the same values as the North and South for the descending pass.

Geological Formation

Sites for CRs and GNSS installations should be located in areas with a stable geological background, free of land deformations, landslides, or other hazardous geological phenomena such as karstic features. Landslide refers to the destabilization of mass layers on a slope and their movement downward and outward [39]. The main causes of landslide creation are (a) geological (e.g., type of lithology), (b) morphological (e.g., tectonic uplift), and (c) human causes (e.g., deforestation) [40].

Table 4. Reclassification of raster layers for the suitability analysis of CRs' sites selection for the ascending and descending orbit directions.

Criteria	Input Values	Output Values (Ascending)	Output Values (Descending)
Slope (degrees)	0 to 5	1	1
	5 to 10	2	2
	10 to 90	3	3
Aspect (degrees)	North (0–22.5)	1	1
	Northeast (22.5–67.5)	1	2
	East (67.5–112.5)	1	3
	Southeast (112.5–157.5)	1	2
	South (157.5–202.5)	1	1
	Southwest (202.5–247.5)	2	1
	West (247.5–292.5)	3	1
	Northwest (292.5–337.5)	2	1
Land Cover	Flat (−1)	3	3
	Tree	1	1
	Bush	2	2
	Soil	3	3
	Rock	2	2
Sigma 0 (dB)	Hard Surface Road	1	1
	−23.38 to −10	1	1
	−10 to 0	2	2
	0 to 5.84	3	3

One of the most hazardous geological phenomena is that of karstic features because they, amongst others, are difficult to detect. The formation of surface and subsurface cavities (e.g., sinkholes) results from karstic processes. The triggering factor of the karstic features is mainly the water and occurs in areas formatted by carbonate rocks (limestone, dolomite and marble), sulphate rocks (gypsum and anhydrites), and halite (salt) sediments [41]. Sedimentation is another hazard that occurs in Cyprus. This phenomenon takes place in areas with expanding soils (e.g., marls and clays), and alluvial soil (i.e., sand, silts, or gravel) areas [42].

Since all the aforementioned types of lithology are problematic in terms of GNSS and CR monumentation, they were excluded from the suitability analysis. The AOI of ALEV is formatted by Sheeted Dykes (Diabase) ophiolite complex of Troodos mountain [43]. Diabase could describe mantle rocks' partial fusion or its fractional crystallization [44]; therefore, regarding monumentation, such material is very convenient.

Boundaries of AOI

DLS provided the boundaries of all the areas of interest after requesting permits to install permanent GPS/GNSS stations and Corner Reflectors. The vector data of the boundaries were used to reduce the suitability analysis results inside the AOI while excluding the unnecessary information—outside of the governmental parcel—acquired from UAV missions, satellite images and GSD geological data.

2.2.3. Analytic Hierarchy Process Analysis (AHP)

Following the reclassification process, the next step is to decide on the allocation of the CR site. Such a decision requires the use of criteria and the selection of alternatives from which a decision must be taken. The alternatives, which, in this case, are subdivisions of the criteria, differ for each criterion because the criteria have varying relevance. Nonetheless, AHP is a mechanism to make such decisions capable of analysing and supporting decisions with many objectives [45]. Saaty [46] has proposed an intensity scale of importance, ranging from 1–9, as a preliminary step for criteria prioritization, as presented in Table 5. Since the hierarchy has been formed, each criterion within every level is compared (judging

their relative importance in pairs) using a pairwise comparison matrix ($[C]$). Judgments (α_{ij}) defined by numbers of the intensity scale are used for the comparison. In a matrix of order n , the number of required judgments is equal to the following:

$$\frac{n \cdot (n - 1)}{2} \quad (3)$$

Table 5. AHP intensity scale of importance [46].

Intensity of Importance	Definition
1	Equal importance
3	Moderate importance
5	Essential or strong importance
7	Demonstrated importance
9	Absolute importance of one over another
2, 4, 6, 8	Intermediate values between the two adjacent judgments

Since it is reciprocal ($\alpha_{ji} = 1/\alpha_{ij}$), the diagonal elements are equal to unity ($\alpha_{ii} = 1$) [45].

After comparing the criteria, a normalized matrix is created based on the division of each element, in every column, by the sum of that column. Each row in the normalized matrix is averaged to determine the most important criterion ($\{w\}$) [47]. Subsequently, the consistency of the ranking is checked calculating the Consistency Index (μ) as the equation, as follows [45]:

$$\mu = \frac{\lambda_{\max} - n}{n - 1} \quad (4)$$

where λ_{\max} is the average of the elements of the consistency vector ($\{C_{\text{consis}}\}$). The latter is a dot product given by the following equation [48]:

$$\{C_{\text{consis}}\} = \{w_s\} \cdot \left\{ \frac{1}{w} \right\} \quad (5)$$

where w_s is the weighted sum vector, and it is calculated by the multiplication of $[C]$ matrix and $\{w\}$.

AHP entails comparing the (μ) of the decision data with the random index (RI) values for consistency check. RI values are the μ estimations expected from a matrix of order of the matrix [49], proposed by Saaty [46]. For instance, RI for order 2 is equal to zero and the value increases with the order of the matrix.

Finally, a consistency check should be performed, calculating the consistency ratio (C_{ratio}), which is defined by the following equation:

$$C_{\text{ratio}} = \frac{\mu}{\text{RI}} \quad (6)$$

A ratio of less than 0.1 indicates consistent judgment, and the generated weights can be applied [50].

The analysis was performed for the criteria (see Table 6) and their values as presented in Tables 7–10. The consistency ratio indicates that the weights produced for AHP analysis can be applied to the WO analysis for the allocation of corner reflectors sites.

Table 6. Pairwise comparison matrix for the criteria weights with respect to the goal.

	Slope	Aspect	Land Cover	Sigma 0	Weight
Slope	1	2	0.5	0.2	0.13
Aspect	0.5	1	0.33	0.2	0.09
Land Cover	2	3	1	0.5	0.26
Sigma 0	5	5	2	1	0.52

$\lambda_{\max} = 4.06$, $\mu = 0.02$, $\text{RI} = 0.89$, $C_{\text{ratio}} = 0.01$ (acceptable consistency).

Table 7. Weights of the reclassified values with respect to the Slope criterion.

Slope	1	2	3	Weight
1	1	2	9	0.58
2	0.5	1	9	0.37
3	0.11	0.11	1	0.05

$\lambda_{\max} = 3.05$, $\mu = 0.02$, $RI = 0.52$, $C_{\text{ratio}} = 0.05$ (acceptable consistency).

Table 8. Weights of the reclassified values with respect to the Aspect criterion for the ascending and descending direction, respectively.

Aspect	1	2	3	Weight
1	1	0.14	0.11	0.06
2	7	1	0.33	0.29
3	9	3	1	0.65

$\lambda_{\max} = 3.07$, $\mu = 0.03$, $RI = 0.52$, $C_{\text{ratio}} = 0.07$ (acceptable consistency).

Table 9. Weights of the reclassified values with respect to the Land Cover criterion.

Land Cover	1	2	3	Weight
1	1	0.125	0.11	0.05
2	8	1	0.33	0.31
3	9	3	1	0.64

$\lambda_{\max} = 3.10$, $\mu = 0.05$, $RI = 0.52$, $C_{\text{ratio}} = 0.09$ (acceptable consistency).

Table 10. Weights of the reclassified values with respect to the Sigma 0 criterion.

Sigma 0	1	2	3	Weight
1	1	5	9	0.75
2	0.2	1	3	0.18
3	0.11	0.33	1	0.07

$\lambda_{\max} = 3.02$, $\mu = 0.01$, $RI = 0.52$, $C_{\text{ratio}} = 0.02$ (acceptable consistency).

2.2.4. Weighted Overlay Analysis (WO)

AHP analysis was performed to derive priority scales for use in WO analysis. The latter is defined as the process of creating a map by overlaying multiple raster layers and assigning a weight to each raster layer (criterion and its values) based on its importance [51]. The method is used to combine standardised components, in which each cell value is multiplied by the percentage weight of the criterion, and the results are added together to succeed in the creation of an output raster according to the following equation [25]:

$$\text{Suitability} = \sum \omega_i \times x_i \quad (7)$$

where ω_i is the weight assigned to each criterion and x_i is the standardized score of each criterion's evaluation scale (0 to 9).

The selection of the input rasters that will be used in the analysis is the first step in the process. As a result, all reclassified rasters that were assessed with the AHP analysis were included in the WO. The next step involves the selection of an evaluation scale for the assignment of the values of each raster. The range of the scale in WO was chosen to be the same as the intensity scale in AHP, which is determined from 1 to 9. Since the evaluation scale has been selected, the cell values for each input raster in the analysis are assigned values according to their importance. All the unwanted values are excluded from the analysis by setting the scale value to Restricted [52]. In the final step, each input raster is assigned an influence percentage based on its importance.

For instance, the sigma 0 raster layer is given a weight of 52% influence, and its reclassified output value 1 (input values -23.38 dB to -10 dB) is assigned a standardized scale value of 8. The Land Cover raster layer has a weight of 26% influence, and its reclassified

output value 3 (input value Soil) is assigned value 6. Consider the rasters overlaid, then the cell values for the inputs mentioned above are transformed into the following:

$$(8 \times 0.52) + (6 \times 0.26) = 4.16 + 1.56 = 5.72$$

However, the output raster from the WO analysis is integer; thus, the final output value is rounded to 6 [53]. Table 11 describes the percentage influence and the standardized scale values for each raster layer participating in the suitability analysis.

Table 11. Raster layers participating in WO analysis. The weights of the criteria and the assigned scale values are derived from AHP analysis.

Criteria	Weight (%)	Input Values	Scale Value
Slope	13	1 (0 to 5)	6
		2 (5 to 10)	4
		3 (10 to 90)	Restricted
Aspect (for ascending pass)	9	1 (N, NE, E, S, SE)	Restricted
		2 (NW, SW)	3
		3 (W, Flat)	7
Land Cover	26	1 (Tree, RoadHs)	Restricted
		2 (Rock, Bush)	3
		3 (Soil)	6
Sigma 0	52	1 (−23.38 to −10)	8
		2 (−10 to 0)	2
		3 (0 to 5.84)	Restricted

The output product of the WO is a weighted raster layer illustrating all the candidate and restricted locations throughout the broader area, determining suitable CR sites in the candidate area of interest. The candidate locations were classified from the most to the least favourable as presented from darker to lighter blue colours in Figure 12.

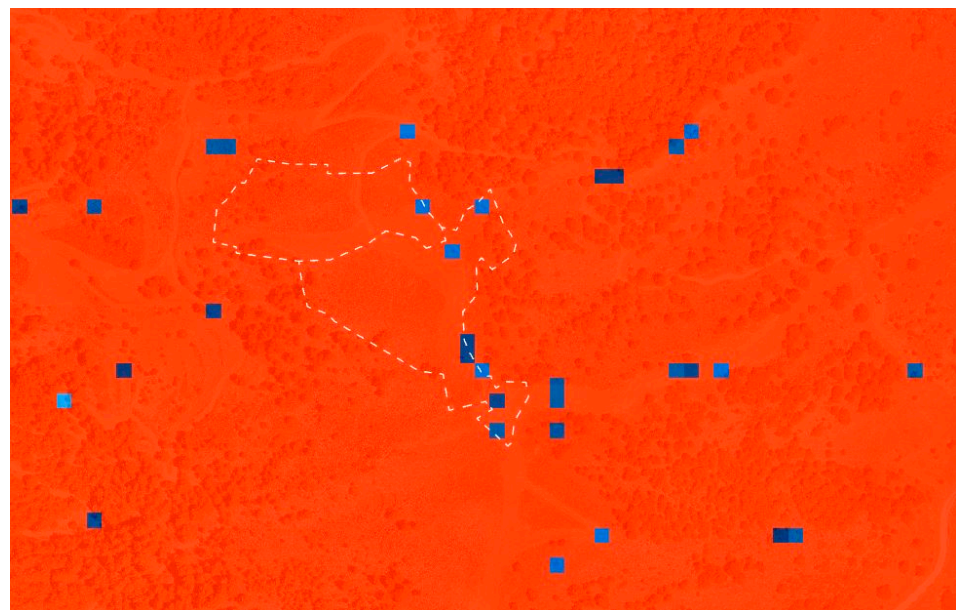


Figure 12. The weighted raster layer illustrates the candidate locations for the monumentation of CR for the ascending pass. The restricted areas are red in colour, and colour ranging from light blue to darker blue indicates suitable locations from the least to the most favourable, respectively. The white dashed polygons determine the boundaries of the AOI.

Nonetheless, candidate sites must be located and selected within the AOI; thus, the area of the candidate locations was substantially reduced by applying constraints of the underlying geology and the boundaries of the AOI (see Figure 13).



Figure 13. The candidate locations inside the AOI boundaries. (a) CR candidate sites for the ascending pass; (b) CR candidate sites for the descending direction.

Weighted Overlay analysis chose the exact positions for both the ascending and descending passes; nevertheless, the cells differ in terms of suitability scale. The latter occurs because all parameters and constraints are fulfilled (i.e., flat terrain and aspect, land cover of soil) at the exact locations except the Sigma 0 criterion, which is the cause of the disparities in cells' values between the ascending and the descending candidate locations.

The two most favourable locations are illustrated in darker blue, and the final location would be chosen if there were no more constraints to consider, such as the following:

- (a) the distance between the 2 CRs;
- (b) the distance between the CRs and the GNSS site;
- (c) the distance from metallic structures;
- (d) the viewshed of the CRs concerning the satellite average incidence angle.

2.3. Visibility Analysis

Beginning from the most favourable locations, if at least one of the aforementioned constraints is not satisfied, the assessment for the optimal site continues to the less convenient location and so on.

At first glance, when looking at the orthomosaic, it is noticeable that there is a metallic boundary fence between the two most ideal locations, 9 m away from the southern deeper blue cell and 14 m away from the northern. Hence, the two darker blue coloured cells are excluded from the selection. Subsequently, the next option—the southern cell for the ascending pass—is selected for the analysis. Simultaneously, the following option for the descending pass site is one of the three light blue coloured cells. Due to the proximity to the GNSS station, the suitable location is chosen to be the northwest light blue cell.

Performing exploratory 3D analysis in ArcGIS Pro software, one of those locations is chosen to be the final. As mentioned, the distance between the two CRs must exceed 200 m, so an elevation profile was carried out (see Figure 14) to check this constraint.

Finally, a visibility analysis was performed for the two CR sites, one for each pass, based on the average incidence angle as described in Table 12.

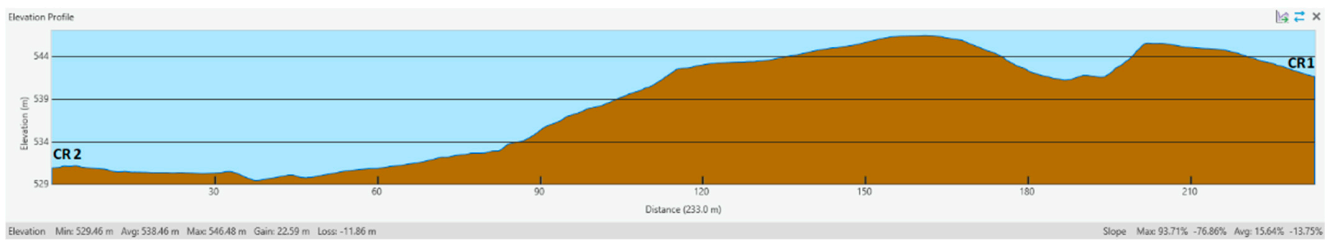


Figure 14. The elevation profile of the two CRs in ALEV location. The distance between them is 230 m. CR1 is referred to the site of the ascending pass and CR2 to the descending.

Table 12. The average incidence angle and the sigma 0 value for the two locations. The data were acquired using Sentinel-1 SLC products from August to September 2020.

Location	Absolute Orbit	Direction and Relative Orbit	Average Incidence Angle	Average Sigma 0 (dB)
Corner Reflector 1	23,286	Ascending (160)	39.7°	−10.65
Corner Reflector 2	23,293	Descending (167)	39.22°	−11.53

Concerning the relative orbits of each pass, and assuming that all SAR sensors have a line of sight that is perpendicular to the satellite platform's travel direction [22], the CR1 was oriented at a 260° azimuth angle, whereas the CR2 has a 100° azimuth angle. As described in Section 2.1.2, to succeed the maximum RCS, for a given incidence angle of ~40°, the CR for ascending pass should have a baseplate elevation angle of ~15°. Figure 15 illustrates the viewsheds in a 3D model, while in Table 13 the viewshed parameters of the CR are described.

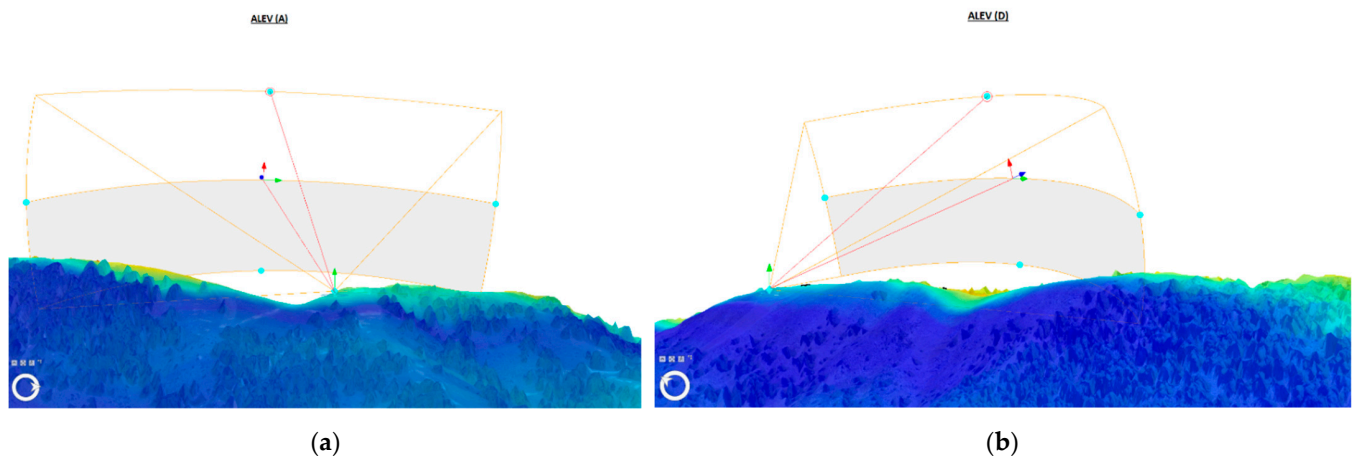


Figure 15. Viewshed perspective of the candidate sites with sigma 0 values overlaid on the terrain. Red lines demonstrate the open face orientation angle of 45°. The lower red line illustrates the baseplate line of sight when CR is tilted at a specific angle. The upper red line points at the line of sight at an elevation angle of 35.26°. (a) viewshed perspective of the CR for the ascending pass; (b) 3D viewshed of the CR for the descending direction.

Table 13. The viewshed parameters for both CRs to succeed maximum RCS.

Viewshed Information	Data
Viewpoint	CR for ascending pass
Azimuth	260°
Baseplate elevation angle	15°
Total elevation angle of CR	51°
Viewpoint	CR for descending pass
Azimuth	100°
Baseplate elevation angle	16°
Total elevation angle of CR	51°
Open face orientation angle	45°
Open face elevation angle	35.26°

Determination of Candidate Locations for GNSS

An exploratory 3D analysis was performed in GIS environment to check the visibility of the GNSS antenna as depicted in Figure 16, and the distance between the GNSS antenna and the 2 CRs (see Figures 17 and 18).

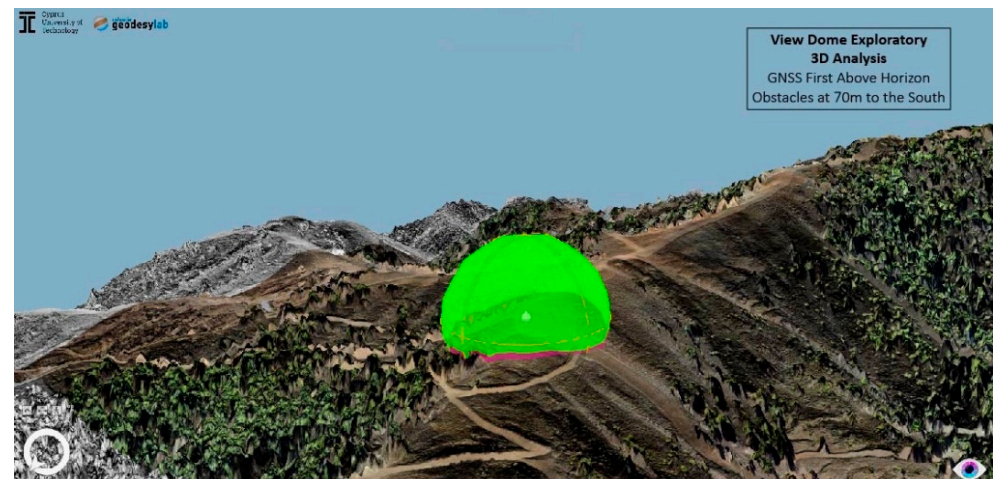


Figure 16. The View Dome visibility analysis of the GNSS antenna illustrates its visible volumetric spaces in 3D. The height of the antenna was determined at 2 m, and the horizontal orange line indicates the elevation cut off angle of 0 degrees. Thus, all obstructions above that line prevent the signal from being received directly at a certain elevation angle.

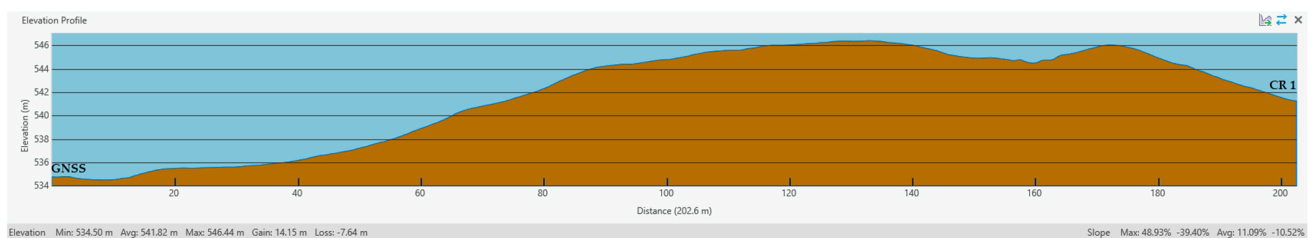


Figure 17. The elevation profile between the GNSS antenna and the CR for the ascending pass. The distance between them is over 200 m.

The closest obstruction was found at 70 m (>30 m) to the South of the GNSS antenna. Nonetheless, this was the most suitable site because of the lack of nearby trees. Furthermore, the aforementioned obstruction was calculated to be 5 degrees above the antenna reference point (ARP) horizon. Therefore, signals can reach the GNSS antenna uninterrupted or unreflected, increasing the likelihood of a reliable position estimate [54].

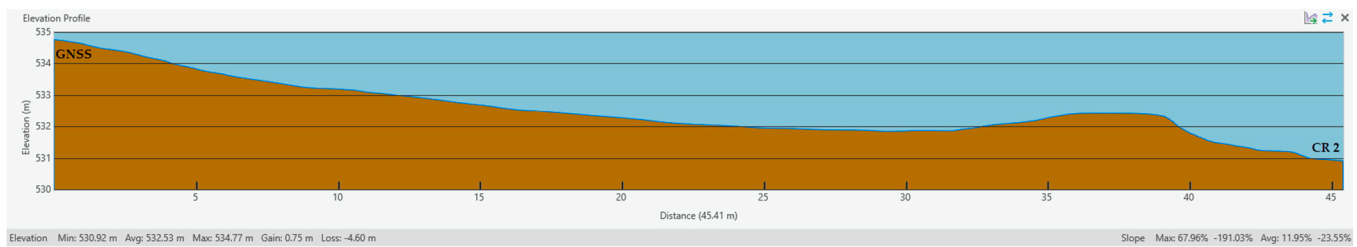


Figure 18. The elevation profile between the GNSS antenna and the CR for the descending pass. The distance between them is 45 m, greater than the constraint of 30 m.

3. Results

3.1. Final Locations of the Co-Located GNSS/SAR Infrastructure

The corner reflectors and GNSS antenna collocation was determined due to the MCDA, described in the previous sections. The inter-visibility between the GNSS antenna and the two corner reflectors was the last consideration to examine; thus, an LOS analysis was performed in the GIS environment, as illustrated in Figure 19. The LOS can define the visibility of sight lines of the instruments over obstacles composed of the DSM.

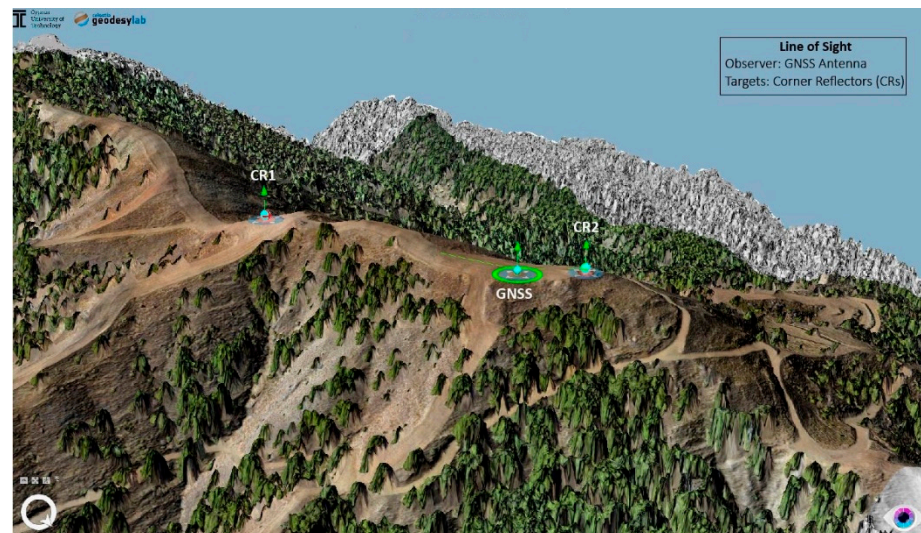


Figure 19. The Line of Sight between GNSS antenna and the two CRs.

The LOS analysis showed that the three instruments had obstructed sightlines, ergo, no inter-visibility. Hence, the suitability analysis for the selection of the most suitable locations was ended, and the sites were finalized.

The subsequent phase of installing the collocated configurations, along with evaluating and validating the sites in terms of signal quality, are described below.

3.2. Installation of GNSS CORS and Corner Reflectors

Following the application of the proposed methodology, a campaign for the installation of the GNSS CORS and corner reflectors begun. In total, twelve CRs and six CORS were installed in six AOI. In particular, the instrumentation of each location includes: (a) two triangular trihedral corner reflectors (one for each pass) of 1.5 m inner dimension, (b) an individually calibrated GNSS geodetic grade antenna (Trimble® GNSS-Ti v2 Choke Ring, Sunnyvale, CA, USA) equipped with radome, (c) a GNSS receiver (Trimble® Alloy, Sunnyvale, CA, USA), (d) a tiltmeter (Jewell D711-A-S, Manchester, NH, USA), (e) a weather station (VAISALA PTU307, Helsinki, Finland) and (f) a solar panel that provides power supply to gel batteries, which are housed inside of an stainless steel enclosure.

The GNSS monument was implemented using the shallow-drilled braced monumentation (SDBM) type [55], which is composed of four solid stainless steel rods (304) anchored at a drilling depth of 2 m—using one of the highest-quality epoxy resins—to form a quad-pod. The GNSS antenna was mounted on an SCIGN mount, the highest standard for permanently mounting GNSS antennas [56], levelled and oriented to True North [57].

The corner reflector's base was installed on top of a layer of reinforced concrete and was anchored with three stainless steel rods at a depth of 1 m, using the same epoxy resin fastening as the GNSS monumentation. The CRs were oriented and levelled towards Sentinel-1 satellite's pass (ascending and descending) line of sight, using a Brunton® Axis Transit compass ($\pm 0.5^\circ$), thus, increasing the likelihood of achieving the highest degree of RCS values. Finally, appropriate fencing was installed to mitigate animal disturbances and unauthorized access. An example of a collocation is shown in Figure 20.



Figure 20. The ALEV site's GNSS and CR (for the descending pass) collocation.

3.3. Site Assessment

3.3.1. Evaluation of CRs Sites

All the CR sites were evaluated with respect to normalized RCS. The theoretical maximum RCS (RCS_T) at C-band of a triangular trihedral CR of 1.5 m is equal to 38.378 dbm² and is derived by the following equation [58]:

$$RCS_T = \frac{4\pi\alpha^4}{3\lambda^2} \quad (8)$$

where α is the inner-length dimension of the CR and λ is the signal's wavelength.

The backscatter coefficient (σ^0) of a distributed target is the ensemble average of the RCS in decibels per illuminated area (A), as follows [59]:

$$\sigma^0 = \frac{RCS}{A} \quad (9)$$

The illuminated area can be calculated using the following equation [22]:

$$A = \frac{\rho_r \cdot \rho_a}{\sin\theta} \quad (10)$$

where ρ_r and ρ_a are the slant range and azimuth pixel spacing, respectively, and θ is the local incidence angle. Therefore, the normalized RCS of any point target in a SAR image can be estimated using the equations mentioned above. Garthwaite et al. [22] noted that an RCS of 34–38 dbm² using an SAR image of coarser beam modes (e.g., IW swath) at C-band, is the suitable range for a CR of 1.5 m.

The evaluation process started on 16 June 2021, with the RCS of each CR extracted from the converted sigma 0, using thirty SAR pictures of ascending and descending orbit directions, respectively. Sentinel-1A and B SLC products with IW swath mode and VV polarization were analysed using SNAP software. The average normalized RCS for each CR is presented in Table 14.

Table 14. The average normalized RCS values derived from each CR in each location.

Site	CR ID	Average RCS (dBm ²)	Difference ¹ (dBm ²)
SOUN	1	35.61	2.77
	2	35.69	2.69
MATS	1	34.24	4.14
	2	35.27	3.11
TROU	1	34.25	4.13
	2	35.17	3.21
ALEV	1	34.22	4.16
	2	34.19	4.19
AKMS	1	34.43	3.95
	2	35.33	3.05
ASGA	1	34.81	3.57
	2	34.72	3.66

¹ The difference between the theoretical peak RCS and the average normalized RCS values.

A representative example of the backscatter coefficient before and after the CRs installation is illustrated in Figure 21.

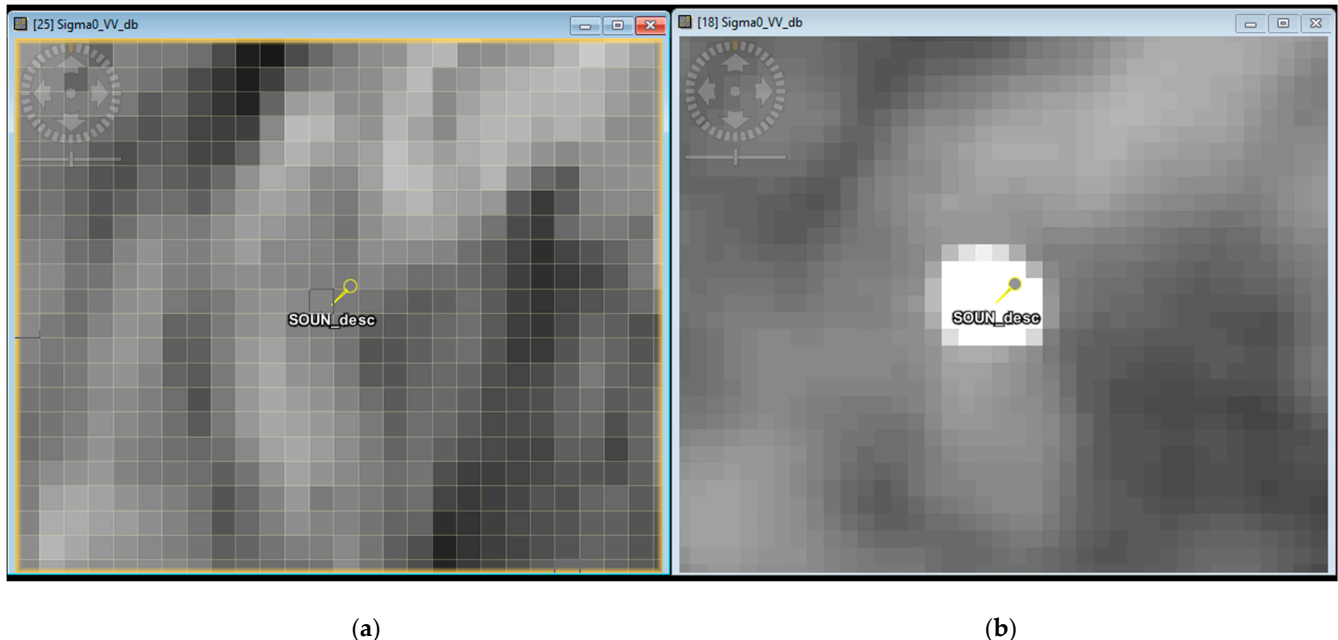


Figure 21. The sigma 0 of the CR for the descending pass in the SOUN site. The RCS was calculated at 36.79 dBm². (a) The backscatter coefficient before the CR installation and (b) after the CR installation.

3.3.2. Evaluation of GNSS CORS Sites

The requirements needed for a GNSS permanent station to fulfil, in order to participate in applications such as crustal motion monitoring, are strict, and the attributes that any agency sets are pretty similar (e.g., visibility, stability, instrumentation) [1]. Amongst others, a reference station is considered stable if coordinate changes do not exceed 10 mm

horizontally and 15 mm vertically in 24 h [54]. Moreover, the receiver should track at least ten satellites above the elevation cut off angle of 0 degrees [60].

An example of satellite availability and horizontal stability is given in Figures 22 and 23, respectively, representing the ALEV GNSS permanent station. At first glance, the evaluation indicates that the GNSS site fulfils the criteria, hence, the goal of the suitability analysis was achieved.

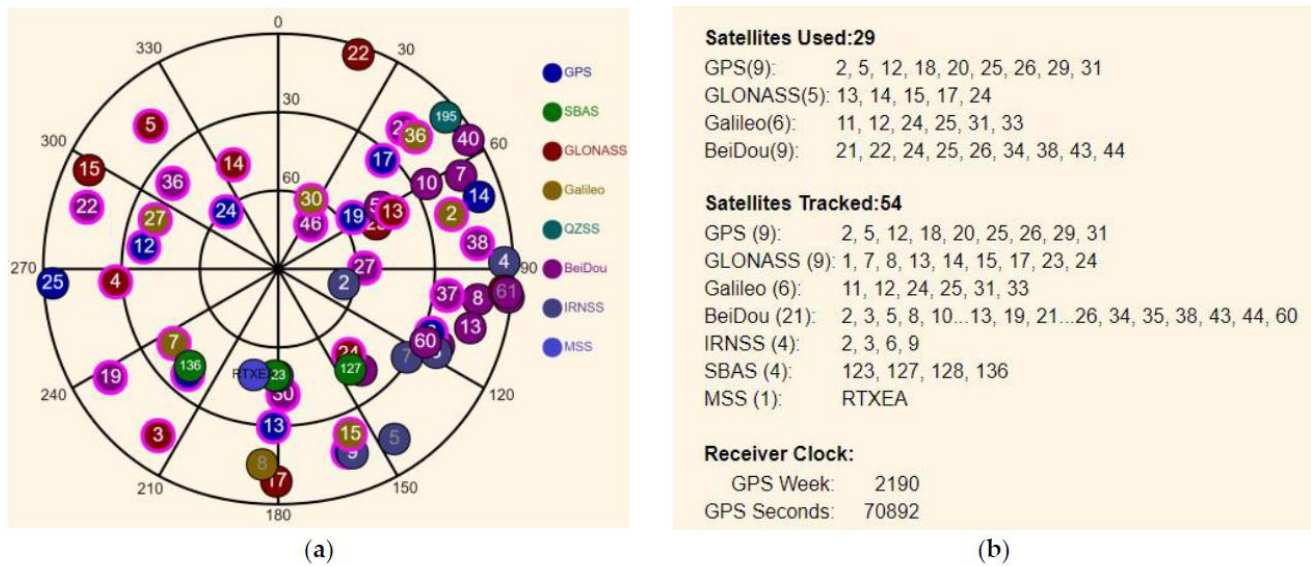


Figure 22. Satellite availability in ALEV GNSS permanent station. (a) The skyplot of the GNSS constellation; (b) The number of satellites tracked and used by the GNSS receiver.



Figure 23. The horizontal stability of the ALEV GNSS monument in 24 h observations.

4. Discussion

The CyCLOPS network is the first strategic infrastructure, deployed at a national scale, dealing with the collocation of two CRs (one for each pass direction), with a permanent GNSS station. The Multi-Criteria Decision Analysis for the collocated infrastructure must be carried out so that the instruments' installation and performance follow the literature guidelines and requirements set by global authorities. The GNSS should be installed on bedrock, at a location with high visibility, to ensure both high stability and satellite availability. Furthermore, the two CRs should be installed in such a way as to achieve the maximum RCS, while at the same time, the GNSS signal is not affected by unwanted multipath.

The main criteria for selecting the most suitable location for installing a CR are sigma 0, slope, aspect, and land cover. Sigma 0 was acquired from SAR images, whilst the rest of the criteria were created using the final products from the UAV missions. Furthermore, the geology formation and the boundaries of the AOI were used as constraints in the site suitability analysis process. The criteria and their values were categorized based on their relative importance and influence on achieving the goal (i.e., the most suitable locations).

The sigma 0 was selected as the criterion of the strongest importance, whilst the remaining criteria, which influence the performance of sigma 0, were categorized as criteria with lower importance. For instance, if an area includes dense vegetation, exposed rocks, and flat terrain, the clutter will be higher than if it comprises a proper slope ($<10^\circ$) without vegetation or soil (large slope causes high backscattering due to the foreshortening effect). Therefore, the land cover criterion is the second priority in the intensity scale, and the slope is the third. The criterion with the weakest importance is the terrain aspect, which determines where the slope is facing. Nevertheless, this information is helpful because areas with a low sigma 0 are usually obscured from satellite LOS and, thus, have a low backscattering coefficient. As a result, if such a location is chosen for CR installation, the latter is unlikely to have LOS with the satellite.

The AHP and WO methods, along with 3D visibility analysis, were used for the suitability analysis. In more detail, AHP was performed to derive priority scales for use in WO, while the latter was used for the image production and extraction of the candidate locations. Finally, the 3D visibility analysis was performed to finalize the most suitable locations.

The installation of the CRs at the sites resulted in RCS values greater than 34 dBm^2 on average. Similarly to the CR results, the evaluation of GNSS sites demonstrated sufficient daily horizontal stability (coordinate changes $\leq 10 \text{ mm}$ in 24 h) and satellite availability (>10 satellites above the elevation angle of 0°).

The results are fully aligned with all the requirements derived from the current scientific literature. This fact indicates that the installation of collocated GNSS CORS and dual CR permanent infrastructures, via the proposed methodology, is successful at first glance. It is worth highlighting that some of the criteria used for this research are not mandatory, since the factors differ from area to area. For instance, if an AOI is plain, the slope and aspect criteria can be ignored.

5. Conclusions

This research revolved around the presentation of a new, semi-automatic process, to determine the most locations for the collocation of GNSS CORS, with InSAR CRs in the framework of the establishment of strategic permanent infrastructures. The proposed methodology involves three major steps; the criteria were derived from the guidelines set by international authorities on GNSS and the current scientific literature on CR installation. Consequently, the criteria were used in the MCDA analysis to determine candidate locations. Finally, candidate locations were reduced by means of the 3D visibility analysis.

The proposed methodology was successful in evaluating the framework of the CyCLOPS project, which involved the establishment of six permanent collocated GNSS CORS and dual CR stations. The evaluation process showed that the methodology is successful,

and the results are fully aligned with the authority and scientific requirements set for the installation of such sensors.

Author Contributions: Conceptualization, C.D.; methodology, D.K. and C.D.; validation, D.K., K.F. and C.D.; formal analysis, D.K. and K.F.; investigation, D.K., K.F., G.M. and C.D.; resources, C.D. and G.M.; writing—original draft preparation, D.K.; writing—review and editing, D.K. and C.D.; visualization, D.K.; supervision, C.D.; project administration, C.D.; funding acquisition, C.D. All authors have read and agreed to the published version of the manuscript.

Funding: This paper is funded by the Cyprus University of Technology Open Access Author Fund. D.K. and K.F. were financially supported by the CyCLOPS (RIF/INFRASTRUCTURES/1216/0050) project (<https://cyclops.cy>, accessed on 28 December 2021), which was co-funded by the European Union Regional Fund and Republic of Cyprus through the Research and Innovation Foundation.

Institutional Review Board Statement: Not Applicable.

Informed Consent Statement: Not Applicable.

Data Availability Statement: Copernicus Sentinel data 2021. Retrieved from ASF DAAC 16 June 2021, processed by ESA.

Acknowledgments: The authors would like to acknowledge the ‘CyCLOPS’ (RIF/INFRASTRUCTURES/1216/0050) project (cyclops.cy), which is co-funded by the European Regional and Development Fund and the Republic of Cyprus through the Research and Innovation Foundation in the framework of the RESTART 2016–2020 programme. The authors would like to acknowledge the ‘EXCELSIOR’ H2020 Teaming project (www.excelsior2020.eu, accessed on 28 December 2021). This paper is under the auspices of the activities of the ‘ERATOSTHENES: Excellence Research Centre for Earth Surveillance and Space-Based Monitoring of the Environment’, ‘EXCELSIOR’ project, that has received funding from the European Union’s Horizon 2020 research and innovation programme, under Grant Agreement No. 857510, and from the Government of the Republic of Cyprus through the Directorate General for the European Programmes, Coordination, and Development.

Conflicts of Interest: The authors declare no conflict of interest.

References

1. Kakoullis, D.; Danezis, C. Permanent Infrastructures for Continuous Space-Based Monitoring of Natural Hazards. In Proceedings of the Eighth International Conference on Remote Sensing and Geoinformation of the Environment (RSCy2020), International Society for Optics and Photonics, Paphos, Cyprus, 26 August 2020; Volume 11524, p. 115241F.
2. Staudacher, T.; Peltier, A. Ground Deformation at Piton de La Fournaise, a Review From 20 Years of GNSS Monitoring. In *Active Volcanoes of the Southwest Indian Ocean: Piton de la Fournaise and Karthala*; Bachelery, P., Lenat, J.-F., Di Muro, A., Michon, L., Eds.; Active Volcanoes of the World; Springer: Berlin/Heidelberg, Germany, 2016; pp. 251–269, ISBN 978-3-642-31395-0.
3. Yu, X.; Hu, J.; Sun, Q. Estimating Actual 2D Ground Deformations Induced by Underground Activities with Cross-Heading InSAR Measurements. *J. Sens.* **2017**, *2017*, e3170506. [[CrossRef](#)]
4. Mahapatra, P.S.; Samiei-Esfahany, S.; van der Marel, H.; Hanssen, R.F. On the Use of Transponders as Coherent Radar Targets for SAR Interferometry. *IEEE Trans. Geosci. Remote Sens.* **2014**, *52*, 1869–1878. [[CrossRef](#)]
5. Fuhrmann, T.; Garthwaite, M.; Brennand, S.; Brown, N. Combination of GNSS and InSAR for Future Australian Datums. In Proceedings of the International Global Navigation Satellite Systems Association IGSS Symposium, Sydney, Australia, 7–9 February 2018.
6. Mahapatra, P.; Marel, H.; Van Leijen, F.; Samiei Esfahany, S.; Klees, R.; Hanssen, R. InSAR Datum Connection Using GNSS-Augmented Radar Transponders. *J. Geod.* **2017**, *92*, 21–32. [[CrossRef](#)]
7. Ferretti, A.; Prati, C.; Rocca, F. Permanent Scatterers in SAR Interferometry. *IEEE Trans. Geosci. Remote Sens.* **2001**, *39*, 8–20. [[CrossRef](#)]
8. Danezis, C.; Hadjimitsis, D.G.; Eineder, M.; Brcic, R.; Agapiou, A.; Themistocleous, K.; Mendonidis, E.; Tzouvaras, M.; Hadjicharalambous, K.; Pilidou, S.; et al. CyCLOPS: A Novel Strategic Research Infrastructure Unit for Continuous Integrated Spaced-Based Monitoring of Geohazards. In Proceedings of the 4th Joint International Symposium on Deformation Monitoring (JISDM), Athens, Greece, 15–17 May 2019.
9. ICSM. *Guideline for Continuously Operating Reference Stations—Special Publication 1*; Intergovernmental Committee on Survey and Mapping (ICSM): Canberra, Australia, 2014.
10. Combrinck, L.; Schmidt, M. Physical Site Specifications: Geodetic Site Monumentation. In Proceedings of the IGS Network System Workshop, Annapolis, MD, USA, 2–5 November 1998; p. 8.
11. IGS. *IGS Site Guidelines*; Infrastructure Committee, Central Bureau: Pasadena, CA, USA, 2007; p. 15.

12. Bruyninx, C. *Guidelines for EPN Stations & Operational Centres*; EUREF: Berlin, Germany, 2019; p. 16.
13. Puskas, C.M.; Meertens, C.M.; Phillips, D.A.; Blume, F.; Rost, M. *Introduction to Anubis Software for GNSS Quality Control in the GAGE Facility and NOTA*; UNAVCO: Boulder, CO, USA, 2019.
14. Thankappan, M.; Garthwaite, M.C.; Williams, M.L.; Hislop, A.; Nancarrow, S.; Dawson, J. Characterisation of Corner Reflectors for the Australian Geophysical Observing System to Support SAR Calibration. In Proceedings of the ResearchGate, Edinburgh, UK, 9–13 September 2013.
15. Garthwaite, M.C. On the Design of Radar Corner Reflectors for Deformation Monitoring in Multi-Frequency InSAR. *Remote Sens.* **2017**, *9*, 648. [\[CrossRef\]](#)
16. Brock, B.; Doerry, A. *Radar Cross Section of Triangular Trihedral Reflector with Extended Bottom Plate*; U.S. Department of Commerce, National Technical Information Service: Springfield, VA, USA, 2009.
17. Garthwaite, M.C.; Thankappan, M.; Williams, M.L.; Nancarrow, S.; Hislop, A.; Dawson, J. Corner Reflectors for the Australian Geophysical Observing System and Support for Calibration of Satellite-Borne Synthetic Aperture Radars. In Proceedings of the 2013 IEEE International Geoscience and Remote Sensing Symposium—IGARSS, Melbourne, VIC, Australia, 21–26 July 2013; IEEE: Melbourne, Australia, 2013; pp. 266–269.
18. Crosetto, M.; Monserrat, O.; Cuevas González, M.; Devanthery, N.; Crippa, B. Persistent Scatterer Interferometry: A Review. *ISPRS J. Photogramm. Remote Sens.* **2016**, *115*, 78–89. [\[CrossRef\]](#)
19. Rosenqvist, A.; Perez, A.; Olfindo, N. *A Layman's Interpretation Guide to L-Band and C-Band Synthetic Aperture Radar Data*; Committee on Earth Observation Satellites: Washington, DC, USA, 2018.
20. Freeman, A. SAR Calibration: An Overview. *IEEE Trans. Geosci. Remote Sens.* **1992**, *30*, 1107–1121. [\[CrossRef\]](#)
21. Jauvin, M.; Yan, Y.; Trouvé, E.; Fruneau, B.; Gay, M.; Girard, B. Integration of Corner Reflectors for the Monitoring of Mountain Glacier Areas with Sentinel-1 Time Series. *Remote Sens.* **2019**, *11*, 988. [\[CrossRef\]](#)
22. Garthwaite, M.C.; Nancarrow, S.; Hislop, A.; Thankappan, M.; Dawson, J.H.; Lawrie, S. *The Design of Radar Corner Reflectors for the Australian Geophysical Observing System: A Single Design Suitable for InSAR Deformation Monitoring and SAR Calibration at Multiple Microwave Frequency Bands*; Geoscience Australia: Canberra, Australia, 2015; ISBN 978-1-925124-57-6.
23. Parker, A.L.; Featherstone, W.E.; Penna, N.T.; Filmer, M.S.; Garthwaite, M.C. Practical Considerations before Installing Ground-Based Geodetic Infrastructure for Integrated InSAR and CGNSS Monitoring of Vertical Land Motion. *Sensors* **2017**, *17*, 1753. [\[CrossRef\]](#)
24. ESA. Sentinel-1 SAR Definitions. Available online: <https://sentinels.copernicus.eu/web/sentinel/user-guides/sentinel-1-sar/definitions> (accessed on 13 December 2021).
25. Eastman, J.R. Multi-Criteria Evaluation and GIS. *Geogr. Inf. Syst.* **1999**, *1*, 493–502.
26. Thompson, J.A.; Bell, J.C.; Butler, C.A. Digital Elevation Model Resolution: Effects on Terrain Attribute Calculation and Quantitative Soil-Landscape Modeling. *Geoderma* **2001**, *100*, 67–89. [\[CrossRef\]](#)
27. Al-Rawabdeh, A.; He, F.; Moussa, A.; El-Sheimy, N.; Habib, A. Using an Unmanned Aerial Vehicle-Based Digital Imaging System to Derive a 3D Point Cloud for Landslide Scarp Recognition. *Remote Sens.* **2016**, *8*, 95. [\[CrossRef\]](#)
28. SenseFly Photogrammetry Mapping Drone Camera. Available online: <https://www.sensefly.com/camera/sensefly-soda-3d-mapping-camera/> (accessed on 14 December 2021).
29. ESRI. How Slope Works. Available online: <https://pro.arcgis.com/en/pro-app/latest/tool-reference/spatial-analyst/how-slope-works.htm> (accessed on 16 December 2021).
30. ESRI. How Aspect Works. Available online: <https://pro.arcgis.com/en/pro-app/latest/tool-reference/spatial-analyst/how-aspect-works.htm> (accessed on 17 December 2021).
31. ESA. Sentinel-1 Missions. Available online: <https://sentinel.esa.int/web/sentinel/missions/sentinel-1/satellite-description/orbit> (accessed on 17 December 2021).
32. Liu, P. InSAR Observations and Modeling of Earth Surface Displacements in the Yellow River Delta (China). Ph.D. Thesis, University of Glasgow, Glasgow, UK, 2012.
33. Shakya, A.K.; Ramola, A.; Kandwal, A.; Prakash, R. Comparison of Supervised Classification Techniques with ALOS PALSAR Sensors for Roorkee Region of Uttarakhand, India. *Int. Arch. Photogramm. Remote Sens. Spat. Inf. Sci.* **2018**, *XLII-5*, 693–701. [\[CrossRef\]](#)
34. Ferretti, A.; Monti-Guarnieri, A.; Prati, C.; Rocca, F. *InSAR Principles: Guidelines for SAR Interferometry Processing and Interpretation*; European Space Agency: Noordwijk, The Netherlands, 2007; ISBN 92-9092-233-8.
35. ESA. Sentinel-1 SAR Acquisition Modes. Available online: <https://dragon3.esa.int/web/sentinel/user-guides/sentinel-1-sar/acquisition-modes> (accessed on 19 December 2021).
36. Michelson, D.G.; Jull, E.V. Depolarizing Trihedral Corner Reflectors for Radar Navigation and Remote Sensing. *IEEE Trans. Antennas Propag.* **1995**, *43*, 513–518. [\[CrossRef\]](#)
37. Haynes, D.; Mitchell, P.; Shook, E. Developing the Raster Big Data Benchmark: A Comparison of Raster Analysis on Big Data Platforms. *ISPRS Int. J. Geo-Inf.* **2020**, *9*, 690. [\[CrossRef\]](#)
38. Briney, A. Overview of Weighted Site Selection and Suitability Analysis. Available online: <https://www.gislounge.com/overview-weighted-site-selection-suitability-analysis/> (accessed on 9 March 2021).
39. Efthymiou, M.; Hadjicharalambous, K.; Morisseau, E.G. *Landslides in Cyprus and Their Consequences to the Built Environment*; Geological Survey Department: Nicosia, Cyprus, 2013.

40. Highland, L. *Landslide Types and Processes*; U.S. Geological Survey: Reston, VA, USA, 2004.
41. Hadjicharalambous, K.; Michaelides, P. *Karstic Phenomena*; Geological Survey Department: Nicosia, Cyprus, 2017.
42. Geological Survey Department. *Loose Soils*; Geological Survey Department: Nicosia, Cyprus, 2019.
43. Richardson, C.J.; Cann, J.R.; Richards, H.G.; Cowan, J.G. Metal-Depleted Root Zones of the Troodos Ore-Forming Hydrothermal Systems, Cyprus. *Earth Planet. Sci. Lett.* **1987**, *84*, 243–253. [[CrossRef](#)]
44. Moores, E.M.; Vine, F.J. The Troodos Massif, Cyprus and Other Ophiolites as Oceanic Crust: Evaluation and Implications. *Philos. Trans. R. Soc. Lond. Ser. A Math. Phys. Sci.* **1971**, *268*, 443–467. [[CrossRef](#)]
45. Saaty, T.L. Decision Making—The Analytic Hierarchy and Network Processes (AHP/ANP). *J. Syst. Sci. Syst. Eng.* **2004**, *13*, 1–35. [[CrossRef](#)]
46. Saaty, T.L. A Scaling Method for Priorities in Hierarchical Structures. *J. Math. Psychol.* **1977**, *15*, 234–281. [[CrossRef](#)]
47. Saaty, R.W. The analytic hierarchy process—What it is and how it is used. *Mathl. Model.* **1987**, *9*, 161–176. [[CrossRef](#)]
48. Dieter, G.E.; Schmidt, L.C. *Engineering Design*, 5th ed.; McGraw-Hill: New York, NY, USA, 2013; ISBN 978-0-07-339814-3.
49. Donegan, H.A.; Dodd, F.J. A Note on Saaty’s Random Indexes. *Math. Comput. Model.* **1991**, *15*, 135–137. [[CrossRef](#)]
50. Aydi, A.; Abichou, T.; Nasr, I.H.; Louati, M.; Zairi, M. Assessment of Land Suitability for Olive Mill Wastewater Disposal Site Selection by Integrating Fuzzy Logic, AHP, and WLC in a GIS. *Environ. Monit. Assess.* **2016**, *188*, 13. [[CrossRef](#)] [[PubMed](#)]
51. Basharat, M.; Shah, H.R.; Hameed, N. Landslide Susceptibility Mapping Using GIS and Weighted Overlay Method: A Case Study from NW Himalayas, Pakistan. *Arab. J. Geosci.* **2016**, *9*, 292. [[CrossRef](#)]
52. Malczewski, J. On the Use of Weighted Linear Combination Method in GIS: Common and Best Practice Approaches. *Trans. GIS* **2000**, *4*, 5–22. [[CrossRef](#)]
53. ArcGIS. *Weighted Overlay*; ESRI: Redlands, CA, USA, 2002.
54. Canadian Geodetic Survey GNSS Reference Station Installation and Operation: Best Practices. *Gov. Can.* **2017**, *20*. [[CrossRef](#)]
55. UNAVCO. Shallow Drilled Braced Monument. Available online: <https://kb.unavco.org/kb/article.php?id=301> (accessed on 27 November 2019).
56. UNAVCO GNSS. Antenna Mounts. Available online: <https://kb.unavco.org/kb/article.php?id=394> (accessed on 16 November 2021).
57. IGS. *IGS Site Guidelines*; Infrastructure Committee, Central Bureau: Pasadena, CA, USA, 2015.
58. Li, C.; Zhao, J.; Yin, J.; Zhang, G.; Shan, X. Analysis of RCS Characteristic of Dihedral Corner and Triangular Trihedral Corner Reflectors. In Proceedings of the 2010 5th International Conference on Computer Science Education, Hefei, China, 24–27 August 2010; pp. 40–43.
59. Calabrese, D.; Episcopo, R. Derivation of the SAR Noise Equivalent Sigma Nought. In Proceedings of the EUSAR 2014, 10th European Conference on Synthetic Aperture Radar, Berlin, Germany, 3–5 June 2014; pp. 1–4.
60. NGS. *Guidelines for New and Existing Continuously Operating Reference Stations (CORS)*; NOAA: Silver Spring, MD, USA, 2018; p. 21.